JOURNAL OF GEOPHYSICAL RESEARCH: SPACE PHYSICS, VOL. 118, 823–831, doi:10.1002/jgra.50146, 2013

Dynamics of the foreshock compressional boundary and its connection to foreshock cavities

N. Omidi,[1] D. Sibeck,[2] X. Blanco-Cano,[3] D. Rojas-Castillo,[3] D. Turner,[4] H. Zhang,[5] and P. Kajdič[6]

Received 12 September 2012; revised 13 December 2012; accepted 22 January 2013; published 28 February 2013.

[1] We use several global hybrid (kinetic ions, fluid electrons) simulation runs for steady and time-varying interplanetary magnetic field (IMF) conditions to examine the dynamics of the foreshock compressional boundary (FCB) and its connection to foreshock cavities. The results demonstrate that for steady IMF conditions, the FCB forms and evolves over a long period of time due to the dynamics of the bow shock and ion foreshock. Formation of the FCB is tied to the generation and nonlinear evolution of ULF waves associated with large-amplitude fluctuations in magnetic field and density within the foreshock. As a result, even during steady IMF conditions, the transitions in the magnetic field strength and direction across an FCB evolve. Although the FCB itself is associated with increases in the magnetic field strength and density, these quantities are reduced on the turbulent side of the FCB as compared to the pristine solar wind. Hybrid simulations with time-varying IMF have been performed to examine the relationship between the FCB and foreshock cavities generated under two possible scenarios. In the first scenario, a bundle of field lines connects to an otherwise quasi-perpendicular bow shock and results in the formation of a finite-sized foreshock region that travels with this bundle of field lines as it connects to different parts of the bow shock surface. Two FCBs bound the traveling foreshock region. In the second scenario, solar wind discontinuities cause the IMF cone angle (angle between the IMF and the solar wind flow direction) to vary and thereby modify the foreshock geometry and the position of the FCB. We demonstrate that structures similar to foreshock cavities bounded by FCBs form in both scenarios. We show that the two scenarios cannot be distinguished based on convecting or nonconvecting FCBs. We also demonstrate that depending on spacecraft location and the nature of the solar wind discontinuities, foreshock cavities may be bounded by an FCB on one side and a foreshock bubble on the other.

Citation: Omidi, N., D. Sibeck, X. Blanco-Cano, D. Rojas-Castillo, D. Turner, H. Zhang, and P. Kajdič (2013), Dynamics of the foreshock compressional boundary and its connection to foreshock cavities, *J. Geophys. Res. Space Physics*, *118*, 823–831, doi:10.1002/jgra.50146.

1. Introduction

[2] Early spacecraft observations revealed the presence of an ion foreshock in the region upstream from the Earth's bow shock. This foreshock is populated by ions reflected from the bow shock and leaking outward from the magnetosheath [*Asbridge et al.*, 1968; *Greenstadt et al.*, 1968]. The backstreaming ions can be found upstream from the quasi-parallel portion of the bow shock, where the shock normal makes an angle of ~45° or less with the interplanetary magnetic field (IMF). The backstreaming ions exhibit a variety of velocity distribution functions that range from field-aligned beams to highly scattered and heated distribution functions called diffuse ions [see *Fuselier*, 1995 for a detailed review]. Also, a variety of ULF waves and nonlinear structures such as foreshock cavitons have been observed in association with the backstreaming ions [e.g., *Hoppe et al.*, 1981; *Russell and Hoppe*, 1983; *Blanco-Cano et al.*, 2009, 2011 and *Kajdič et al.*, 2011].

[3] In the past, a number of boundaries have been discussed in association with the ion foreshock. One is the boundary separating the pristine solar wind from field-aligned, backstreaming ion beams on magnetic field lines

[1]Solana Scientific Inc., Solana Beach, California, USA.
[2]NASA/Goddard Space Flight Center, Greenbelt, Maryland, USA.
[3]Universidad Nacional Autónoma de México, Mexico City, Mexico.
[4]Institute of Geophysics and Planetary Physics/University of California, Los Angeles, Los Angeles, California, USA.
[5]University of Alaska Fairbanks, Fairbanks, Alaska, USA.
[6]Institut de Recherche en Astrophysique et Planétologie, Toulouse, France.

Corresponding author: N. Omidi, Solana Scientific Inc., 777 S. Pacific Coast HWY, #208, Solana Beach, CA 92075, USA. (omidi@solanasci.com)

2169-9380/13/10.1002/jgra.50146

connected to the bow shock [*Asbridge et al*., 1968; *Gosling et al*., 1978; *Paschmann et al*., 1979; *Bonifazi et al*., 1980a, 1980b]. This boundary is typically referred to as the ion (beam) foreshock boundary. The interaction of the field-aligned ion beams with the solar wind results in the generation of ULF waves which are carried back by the solar wind as they grow in amplitude. As a result, ULF wave activity is not detected at the ion foreshock boundary but at another boundary further downstream, identified as the ULF foreshock boundary [*Greenstadt et al*., 1980]. More recently, *Mazelle et al*. [2003] have identified a third boundary that separates field-aligned ion beams from ion beams with gyrating velocity distribution functions. *Skadron et al*. [1986] used MHD to investigate the structure of the foreshock by modeling it as a planar magnetic flux tube containing the backstreaming energetic plasma. The results show the presence of a boundary ~2 R_E (Earth radii) thick, which is associated with increases in density and magnetic field followed by corresponding decreases. The predicted changes in density and magnetic field associated with this boundary are ~2 cm^{-3} and 1 nT corresponding to ~25% of their background values. *Skadron et al*. [1988] examined the interaction of the energetic protons and MHD waves in the foreshock and located the wave compressional boundary (where ULF waves are compressional) for IMF cone angles of 45° and 25°.

[4] In addition to the ion beams and ULF waves, *Sibeck et al*. [2002] reported another phenomenon associated with the foreshock, namely, the isolated structures known as foreshock cavities. The events can be identified on the basis of narrow regions of enhanced density and magnetic field strength bounding regions in which the density and total magnetic field strength are depressed relative to values in the ambient solar wind. The core region also exhibits enhanced ion temperatures and depressed flow velocities. Foreshock cavities were originally thought to be spatial structures created via solar wind interactions with the backstreaming ions [e.g., *Sibeck et al*., 2002]. The spatial structure corresponds to a bundle of field lines that connect to the bow shock where the backstreaming ions originate. However, *Sibeck et al*. [2008] recently suggested that the events might be associated with the back-and-forth motion of a new foreshock boundary over the spacecraft.

[5] *Sibeck et al*. [2008] presented results from a global hybrid (kinetic ions, fluid electrons) simulation indicating the presence of a new boundary, which they termed the foreshock compressional boundary (FCB). The FCB consists of enhancements followed by decrements in density and magnetic field and is on the fast magnetosonic branch. *Sibeck et al*. [2008] suggested that the back-and-forth motion of the FCB over a spacecraft in response to varying IMF orientations would generate signatures in time series data similar to those observed during foreshock cavities. *Omidi et al*. [2009] used global hybrid simulations to examine the properties of FCBs as a function of solar wind conditions such as the Mach number and IMF cone angle (angle between the IMF and the solar wind velocity). They demonstrated that the plasma and magnetic field perturbations associated with FCBs increase with increasing Mach number and exhibit a steepened, shock-like structure at large Mach numbers. Simulation results indicate that the FCBs are present for a wide range of IMF cone angles. Specifically, when the cone angle is small corresponding to near radial IMF, FCBs form symmetrically around the foreshock. As the cone angle increases, FCBs become asymmetric and only appear on one side of the foreshock. *Omidi et al*. [2009] showed an example of the FCB in the Cluster data. Recently, *Rojas-Castillo et al*. [2012] surveyed Cluster observations to determine the statistical properties of FCBs. Their results reveal that FCBs form for a variety of solar wind conditions (i.e., cone angle and velocity) and are highly nonlinear structures with magnetic field and density perturbation ($\delta B/B_o$ and $\delta n/n_o$) amplitudes around 50% of the ambient values. They also find that, in agreement with hybrid simulations, the foreshock compressional boundary is sometimes a transition region between the pristine solar wind plasma and the foreshock plasma, while at other times, it separates a region with large-amplitude waves (cavitons) from regions with high-frequency small-amplitude waves. Cluster data show that the solar wind flow is decelerated and deflected when crossing the FCB.

[6] In this paper, we use global hybrid simulations to examine the properties of the FCB under steady and time-varying IMF conditions. In particular, we show that during

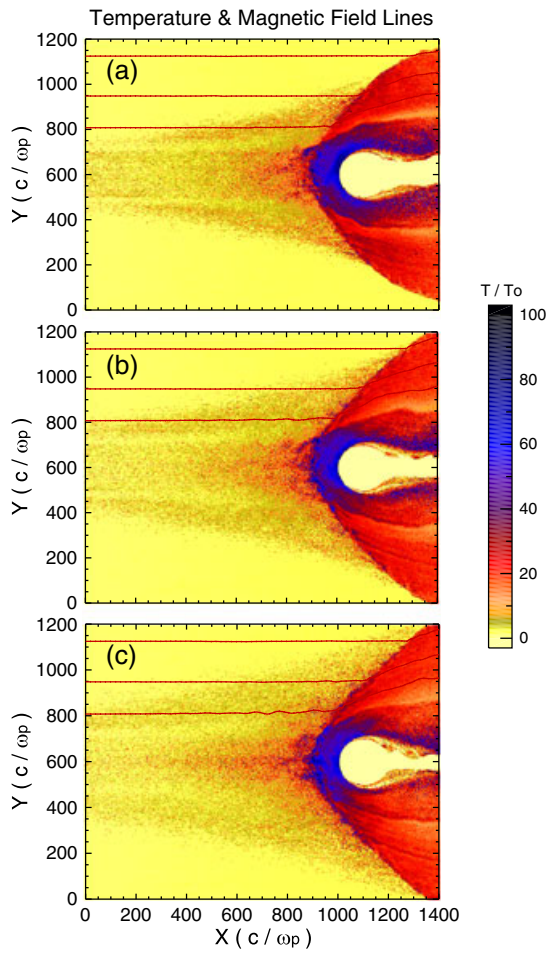

Figure 1. Color intensity plot of ion temperature and magnetic field lines at three times during a run with steady radial IMF shows the evolution of the bow shock and ion foreshock.

steady IMF conditions, the FCB is an evolving structure due to the continued changes in the shape of the bow shock before reaching a steady state. This leads to the formation of new FCBs and the dissipation of the old ones as they are convected into the magnetosheath. Given that prior simulations of FCBs have been under steady IMF conditions [*Sibeck et al*., 2008; *Omidi et al*., 2009), we demonstrate here that FCBs also form during time-varying IMF conditions. We also use the simulations with time-varying IMF to address the generation mechanism of foreshock cavities and examine the viability of the two proposed mechanisms [*Sibeck et al*., 2002, 2008]. We show that both proposed mechanisms are viable and most likely operative under different solar wind conditions. In addition, we show that FCBs are associated with the edges of foreshock cavities under both generation mechanisms.

2. Model

[7] The main tool of investigation in this study is a 2.5-D (2-D in space and 3-D in currents and electromagnetic fields) global hybrid simulation model used extensively in the past [e.g., *Omidi et al*., 2004, 2005, 2006, 2009; *Omidi and Sibeck*, 2007; *Blanco-Cano et al*., 2006, 2009, 2011; *Sibeck et al*., 2008). In electromagnetic hybrid codes, ions are treated as macroparticles and consist of one or more species (e.g., differing mass and charge), whereas electrons are treated as a massless, charge-neutralizing fluid [see, e.g., *Winske and Omidi*, 1993, 1996]. We note that in an earlier study [*Kajdič et al*., 2011], we showed results of 3-D hybrid simulations of FCBs which show a structure very similar to those observed in 2.5-D simulations.

[8] The results presented in this paper are from a number of different hybrid simulation runs under steady or time-varying interplanetary magnetic field (IMF) directions. Here we provide a general description of the model, and the specifics of each run are discussed in the next section. In all cases, a solar wind–type plasma is uniformly loaded in the system and is continuously injected from the left-hand boundary throughout the whole run. The remaining boundaries remain open for the plasma to leave. Similarly, open boundary conditions are applied for the electromagnetic fields so that excited waves and turbulence in the system leave through these boundaries. The bow shock forms in two different ways. In one case, it forms due to the presence of a circular, plasma-reflecting obstacle, and as a result, the run does not include a magnetopause. Therefore, asymmetries associated with magnetopause and the bow shock are

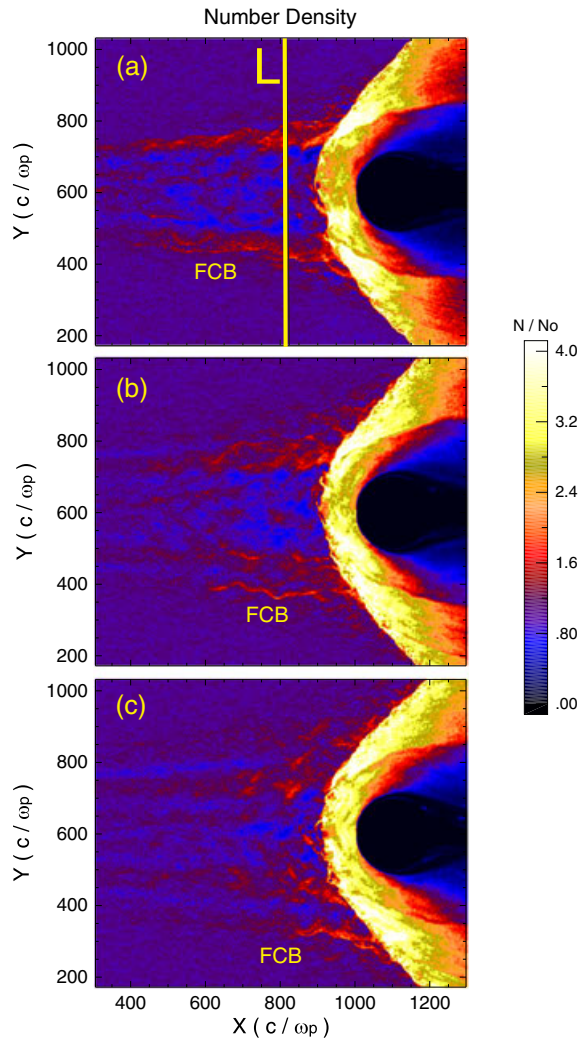

Figure 2. Color intensity plot of density at the same three times as those in Figure 1 shows the evolution of the foreshock compressional boundary.

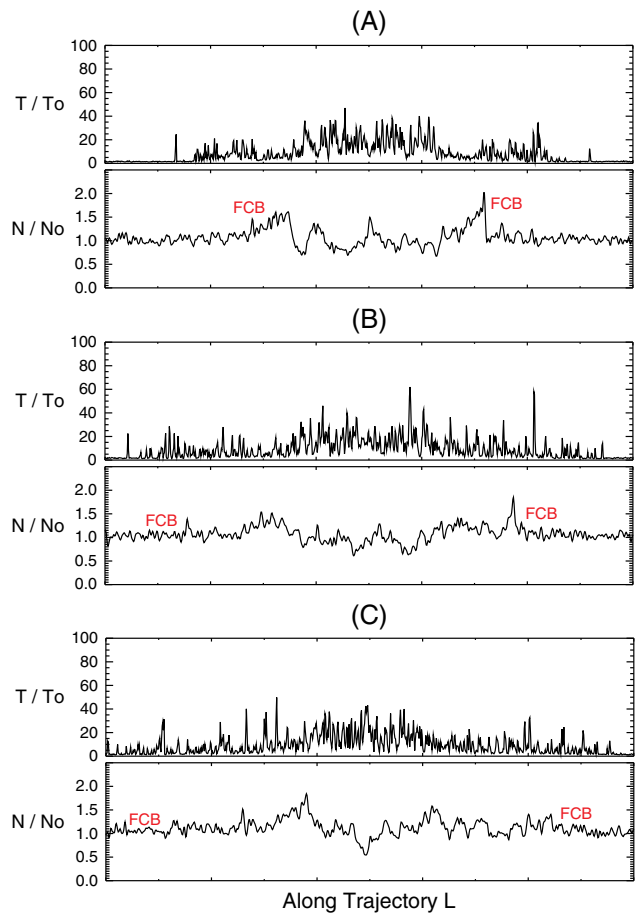

Figure 3. Cuts showing ion temperature and density along trajectory L in Figure 2 at times 100, 125, and 150 Ω_p^{-1}.

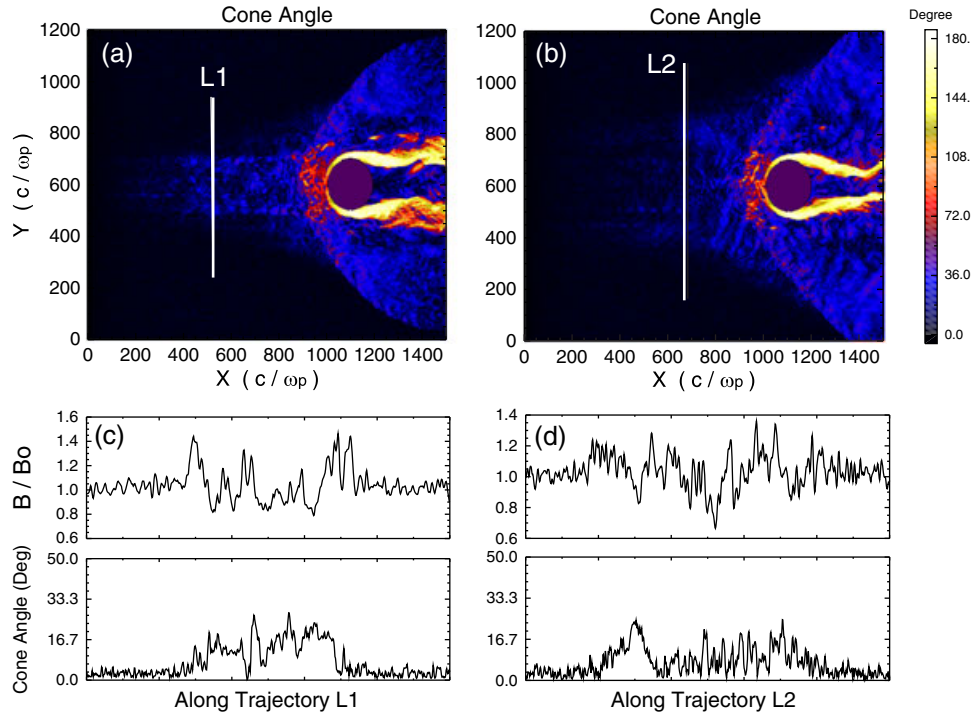

Figure 4. (a, b) Color intensity plot of the IMF cone angle at times 100 and 150 Ω_p^{-1} showing changes in the cone angle across the FCB. (c, d) Variations of the magnetic field strength and the cone angle along trajectories L_1 and L_2.

avoided during radial IMF conditions. In another case, the obstacle to the flow consists of a magnetic dipole inside a circular ionospheric boundary. The simulation box lies in the X–Y (noon–midnight meridian) plane with X along the solar wind flow direction (Sun–Earth line) and the magnetic dipole moment in the Y direction so that X corresponds to $-X_{GSM}$ and Y corresponds to Z_{GSM}. In this study, the simulation box extends a maximum of 2000 ion skin depths c/ω_p (where c is the speed of light and ω_p is the ion plasma frequency) in the X and Y directions with cell size of 1 ion skin depth and 15 particles per cell in the solar wind. To optimize the computational resources, the simulated shocks are smaller (by a factor of ~5) than the Earth's bow shock. On the other hand, the simulated plasma parameters and characteristic time and spatial scales such as gyroperiod, or ion skin depth are the same as in the solar wind. This ensures that the simulations are capable of generating plasma and field values and characteristic scales that can be directly compared to observations at the Earth's bow shock. As demonstrated in our earlier studies, the physical processes occurring in smaller bow shocks and magnetospheres are similar to those at the Earth's magnetosphere, and much can be learned from these simulations, including scaling properties of various magnetospheric processes [e.g., *Omidi et al.*, 2004, 2005, 2006, 2009, 2010; *Omidi and Sibeck*, 2007; *Blanco-Cano et al.*, 2006, 2009, 2011; *Sibeck et al.*, 2008].

3. Simulation Results

[9] In the following, we show results from global hybrid simulations with different IMF geometries. Specifically, in section 3.1, we discuss the results associated with steady, radial IMF geometry, while in section 3.2, we show results

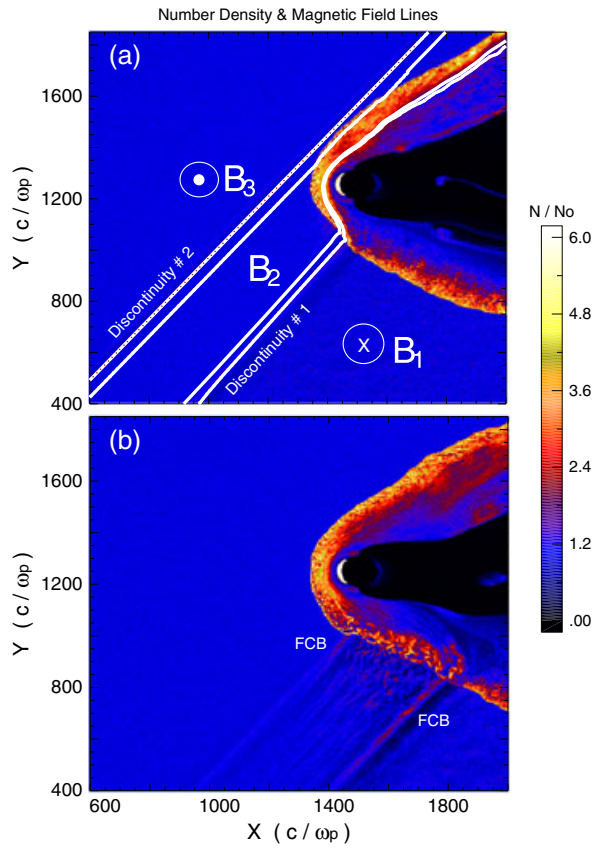

Figure 5. Plots of density at two times during the simulation. (a) Two discontinuities responsible for the changes in the IMF direction during the run. (b) Formation of a convecting foreshock bounded by two FCBs.

from runs with solar wind discontinuities that change the IMF direction in the course of the run.

3.1. Steady IMF

[10] Figure 1 shows the ion temperature (normalized to solar wind value) and selected magnetic field lines at three times (from top to bottom) 100, 125, and 150 Ω_p^{-1} (where Ω_p is the proton angular gyrofrequency) during a run with steady, radial IMF. Similar to the simulations in *Omidi et al*. [2009], the bow shock forms due to the presence of a circular, plasma reflecting obstacle with solar wind Alfven Mach number of 10. In Figure 1, the ion foreshock can be identified on the basis of higher temperatures that results from the presence of energetic backstreaming ions upstream of the bow shock ($X < \sim 900$, $300 < Y < 900$ c/ω_p). Note the enhanced temperatures in the subsolar magnetosheath ($X \sim 1000$, $Y \sim 600$ c/ω_p), which also result from kinetic processes at the quasi-parallel bow shock. The transition from Figures 1a–1c demonstrates that width of the ion foreshock increases with time. Determining if and when the foreshock reaches a steady state would require the use of a 3-D model with a tail sufficiently long enough for the bow shock to reach steady state. In practice, given the time variability of the solar wind, it is unlikely that the bow shock ever reaches a steady state. As such, we expect that FCBs observed by spacecraft are typically not in a steady state but rather dynamic.

[11] Figure 2 shows the plasma density (normalized to solar wind value) at the same times as in Figure 1. Figure 2a shows two foreshock compressional boundaries (FCBs) bounding a turbulent foreshock that exhibits large-amplitude density fluctuations. We note that in 3-D, the FCB has a cylindrical shape as illustrated in *Kajdič et al*. [2011]. Comparing Figures 1 and 2 demonstrates that FCBs do not coincide with the ion beam foreshock boundary, since backstreaming ions are present outside of the FCBs. Figures 2b and 2c show that the broadening of the ion foreshock with time results in the formation of new FCBs at higher latitudes (larger and smaller Y). Solar wind convection carries preexisted FCBs into the magnetosheath, where they dissipate. Here we note that the newly formed FCBs may be associated with smaller amplitudes in density or magnetic field fluctuations as compared to those seen within the foreshock, including those associated with the FCBs formed earlier in the run.

[12] Figures 3a–3c illustrate ion temperatures and densities along the cut labeled "L" in Figure 2a at times 100, 125, and 150 Ω_p^{-1} respectively. In agreement with Figure 2,

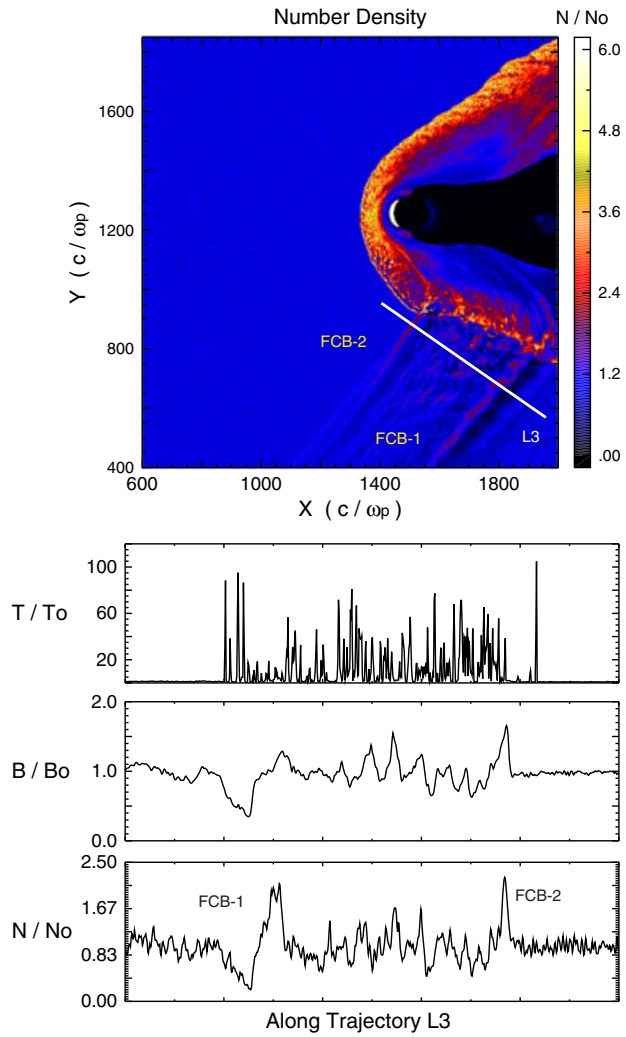

Figure 6. (top) Plasma density and trajectory L_3 that intersects the two formed FCBs. (bottom) Variations of temperature, magnetic field strength, and density along trajectory L_3.

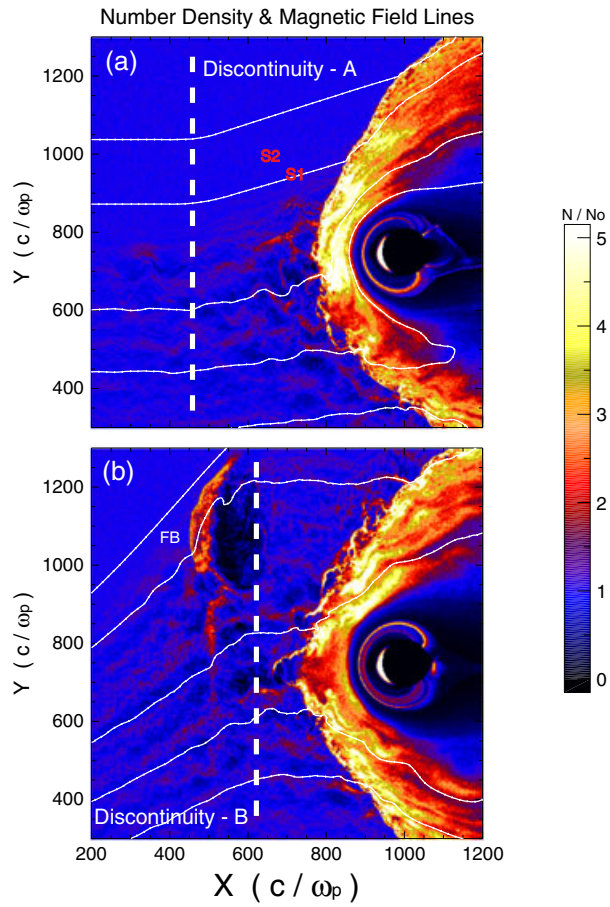

Figure 7. (a) Plots of density and magnetic field lines at two times illustrating discontinuities A and B. (b) Formation of a foreshock bubble downstream of discontinuity B.

the cuts in Figure 3 demonstrate that the FCBs move further apart as the width of the foreshock increases with time. As noted in *Omidi et al*. [2009] and demonstrated in Figure 3, the spatial structure of the FCBs varies considerably in space and time. These results demonstrate that the foreshock compressional boundary is highly dynamic even during steady IMF conditions.

[13] Interestingly, we find that the foreshock compressional boundary marks the location of a rotation in the magnetic field orientation even during steady IMF conditions. The top panels in Figure 4 show color plots of the cone angle in X and Y at times 100 (Figure 4a) and 150 Ω_p^{-1} (Figure 4b). The bottom panels in Figure 4 show the variations of the total magnetic field strength (normalized to solar wind value) and the cone angle along cuts L_1 and L_2 in Figures 4c and 4d, respectively. Whereas the cone angle outside the FCBs is ~0°, it is generally significantly greater than zero inside the FCBs. Consequently, even in the absence of any rotational discontinuities in the solar wind, FCBs are typically associated with rotations in the magnetic field due to the ULF waves and turbulence.

3.2. Time-Varying IMF

[14] In this section, we examine the formation of the FCB for time-varying IMF conditions and describe its relevance to foreshock cavity observations. To this end, we show results from two runs with a magnetic dipole as the obstacle and with time-varying IMF corresponding to the two possible scenarios proposed for the generation/observation of foreshock cavities. The results shown in Figures 5 and 6 are from one of these runs, corresponding to a situation where the two IMF discontinuities illustrated in Figure 5a bound a bundle of field lines connected to the bow shock. Initially, the IMF points in the $-Z$ direction (B_1). Discontinuity #1 rotates the IMF into the X–Y plane at an angle of 45° with the X axis (B_2). Discontinuity #2 then rotates the magnetic field B_2 to align with the $+Z$ direction (B_3). Consequently, the only times and locations where a foreshock can form are those where the bundle of field lines with orientation B_2 between discontinuities # 1 and 2 connect to the quasi-parallel bow shock. As the two discontinuities move antisunward with the solar wind, the foreshock region also convects antisunward. The amplitude of ULF waves within this region grows, leading to the formation of two FCBs marked by enhanced densities shown in Figures 5b and 6a, which correspond to later times in the run. The bottom panel in Figure 6 shows the variations in ion temperature, magnetic field strength, and density along cut L_3 in the top panel in Figure 6. An initial decrease in both density and magnetic field strength followed by an increase in both parameters heralds the arrival of the leading foreshock compressional boundary (FCB-1), which is associated with discontinuity #1. We note that the initial

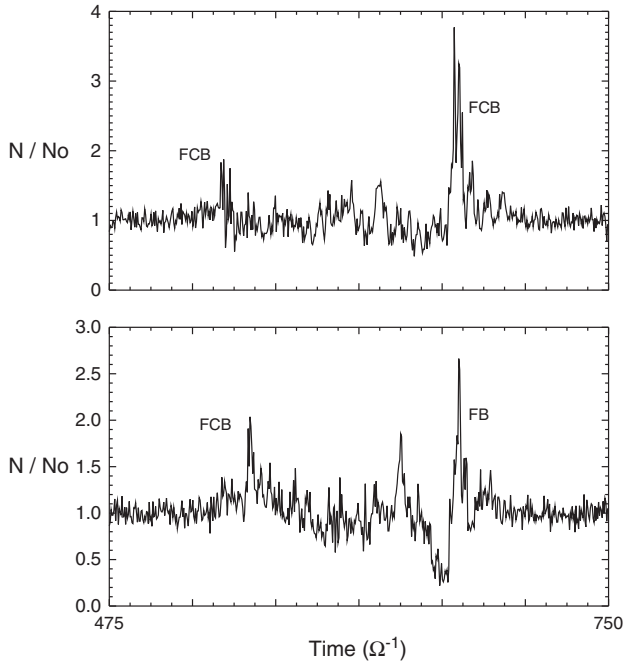

Figure 8. Variation of density with time at (top) $X = 695$, $Y = 930$ and (bottom) $X = 655$, $Y = 970$ showing examples of foreshock cavities bounded by FCB on both sides or a FCB on one side and a foreshock bubble on the other side.

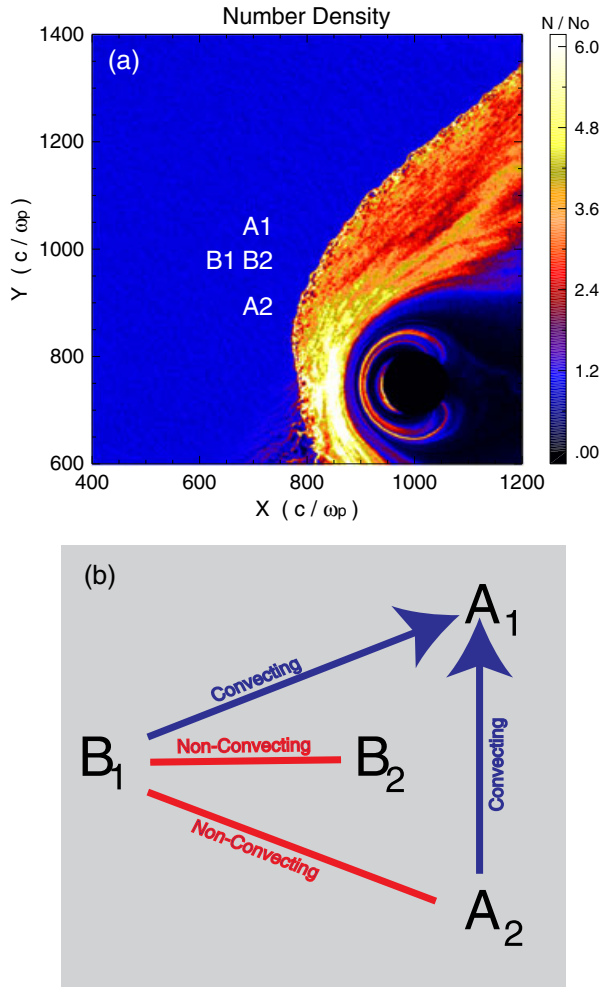

Figure 9. The top panel shows the density and locations of four virtual spacecraft A1, A2, B1, and B2. The bottom panel shows whether comparisons between two spacecraft lead to convecting or nonconvecting foreshock cavity signatures.

decrease in density and magnetic field is associated with the structure of this discontinuity. The results of this run provide support for the idea that foreshock cavities form on bundles of field lines connected to the quasi-parallel bow shock. They also demonstrate that this process is associated with the formation of FCBs and suggest that the density and magnetic field enhancements observed at the edges of foreshock cavities are associated with FCBs.

[15] We have also performed a run with time-varying IMF that allows us to examine the possibility that foreshock cavities result from the back-and-forth motion of FCBs over observing spacecraft. Figure 7a shows the density and magnetic field lines at time 488 Ω_p^{-1} and a rotational discontinuity (RD) labeled A which changes the IMF cone angle from 10° downstream of the RD (on the earthward side) to 0° upstream of the RD (on the sunward side). Figure 7b shows the density and magnetic field lines at time 650 Ω_p^{-1} and a rotational discontinuity labeled B which changes the IMF cone angle from 0° downstream of the discontinuity to 50° upstream of the RD. The interaction of discontinuity B with the backstreaming ions results in the formation of a foreshock bubble (FB) [*Omidi et al.*, 2010], as shown in Figure 7b. Recent analysis of data from THEMIS spacecraft has led to the discovery of foreshock bubbles [*Turner et al.*, 2012].

[16] Figure 8 shows the time variations of density observed by virtual spacecraft at two different locations in the foreshock during this run. The top panel shows the density observed by a virtual spacecraft located at (X = 695, Y = 930 marked by S1 in Figure 7) that is originally in the solar wind and encounters the FCB followed by the foreshock and then has another encounter with the FCB and returns to the solar wind. The bottom panel in Figure 8 shows the density observed by a spacecraft located at (X = 655, Y = 970 marked by S2 in Figure 7) that initially is in the solar wind and encounters the FCB and the foreshock followed by crossing the foreshock bubble formed due to discontinuity B before returning to the solar wind. This result suggests that foreshock cavities may be bounded by FCBs or FBs depending on solar wind conditions and also spacecraft location. The results in Figure 8 demonstrate that the scenario suggested by *Sibeck et al.* [2008] and *Omidi et al.* [2009], namely, the back-and-forth motion of FCB over the spacecraft, can result in signatures in time series data that are consistent with foreshock cavities.

[17] Given that both scenarios proposed for the generation of foreshock cavities seem viable, the question we now address is whether they can be distinguished in spacecraft data. One possible test involves employing multiple spacecraft observations to detect the antisunward moving structures associated with bundles of magnetic field lines connected to the quasi-parallel shock. *Billingham et al.* [2008] reported evidence for such convecting signatures. By contrast, FCBs that simply expand outward or move back-and-forth in response to varying IMF orientations would not be expected to convect antisunward.

[18] To address this question, we examine the signatures expected at four virtual spacecraft A1, A2, B1, and B2 located at positions shown in Figure 9a. Figure 10 shows comparisons for the foreshock cavity signatures observed by pairs of spacecraft A1–A2 and B1–A1 (for the same run shown in Figures 7 and 8). Consistent with convecting

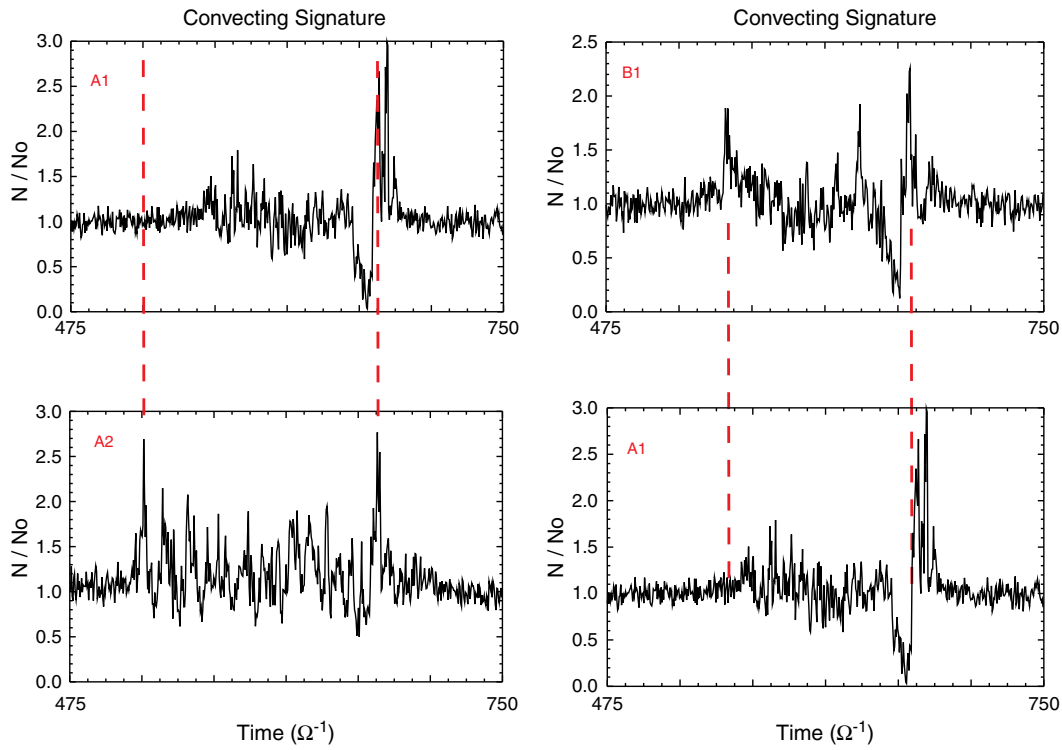

Figure 10. Comparisons between observations of foreshock cavities by spacecraft A1–A2 and A1–B1 shows signatures consistent with convecting structures.

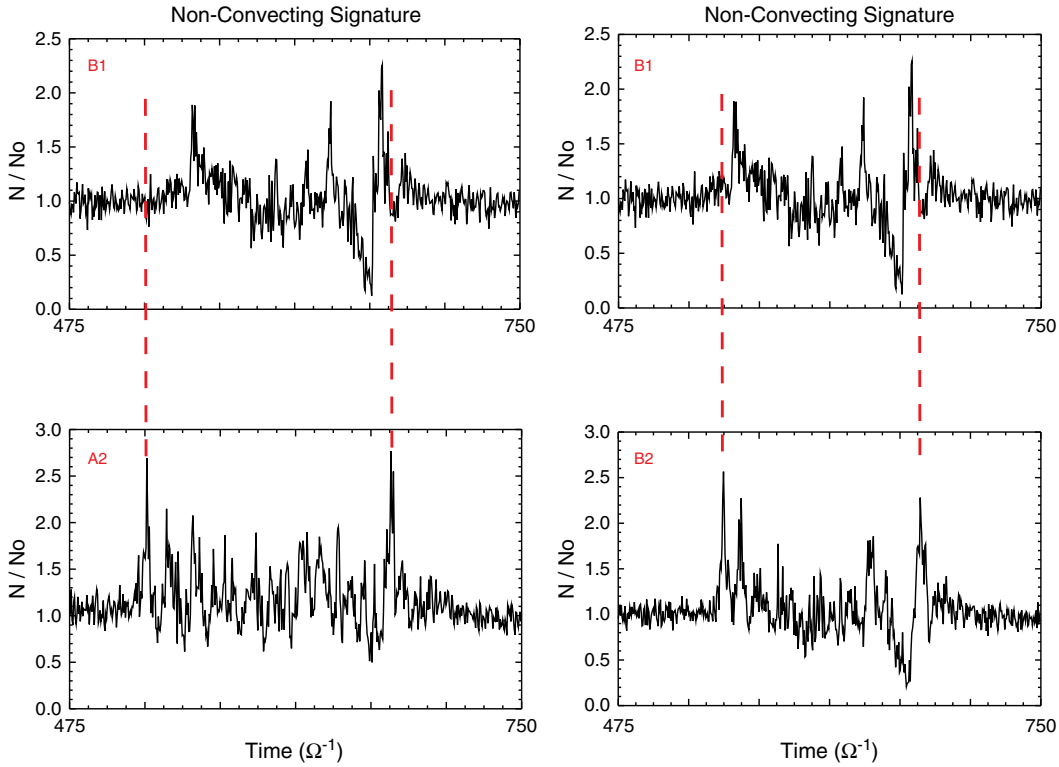

Figure 11. Comparisons between observations of foreshock cavities by spacecraft B1–A2 and B1–B2 shows signatures consistent with nonconvecting structures.

cavities, both spacecraft A2 and B1 enter and leave the cavity before A1. Figure 11 shows comparisons for spacecraft pairs B1–A2 and B1–B2. Both spacecraft A2 and B2 encounter the foreshock cavity before B1, but leave the cavity after B1. These signatures indicate nonconvecting structures. Figure 9b summarizes these results. Due to the dynamic nature of FCBs (as opposed to straight, rigid boundaries), foreshock cavities associated with the back-and-forth motion of FCBs can exhibit both convecting and nonconvecting signatures depending on spacecraft location. As a result, timing methods cannot be used to distinguish between the two generation mechanisms proposed for foreshock cavities.

4. Summary and Conclusions

[19] Using 2.5-D global hybrid simulations, we have examined the properties of FCBs during steady and time-varying IMF conditions. During steady solar wind, the FCB forms well before the bow shock reaches steady state, and as a result, it evolves along with the foreshock. Because the FCB is convected by the solar wind and eventually crosses the bow shock, it must be continuously regenerated. Interaction of FCBs with the bow shock impacts the shock and the magnetosheath plasma with possible magnetospheric consequences. The FCB separates a region of highly turbulent foreshock from either pristine solar wind or ion foreshock with wave activity at much lower amplitudes and higher frequencies as shown by *Rojas-Castillo et al.* [2012]. In the turbulent part of the foreshock, mean values for the density and magnetic field strength are lower than those in the pristine solar wind. The direction of the magnetic field differs from that in the solar wind due to the presence of ULF turbulence and foreshock cavitons. As a result, the IMF cone angle changes across the FCB even in the absence of solar wind discontinuities. This makes it more challenging to determine if any given observed FCB event is associated with the presence of a solar wind discontinuity or not.

[20] Two scenarios for the generation of foreshock cavities were examined and shown to be viable. In one run of the global hybrid code model, a bundle of IMF lines connected to the bow shock resulted in the formation of a convecting foreshock bounded by FCBs. In another run, variations of the IMF with time resulted in the back-and-forth motion of the FCB over the spacecraft, generating time series signatures consistent with foreshock cavities. Since there is nothing unusual about the solar wind input employed for these two scenarios, both likely operate in the foreshock. In both cases, FCBs form and are part of the foreshock cavity structure. The results also show that foreshock cavities formed due to the back-and-forth motion of the FCB may have either convecting or nonconvecting signatures. Therefore, this property of foreshock cavities by itself cannot distinguish between the two possible generation mechanisms. The two mechanisms, however, have much in common in terms of foreshock-related processes such as nonlinear evolution of the ULF waves and formation of FCBs. Finally, we have demonstrated that depending on the nature of the IMF discontinuity, a foreshock bubble may also form and be a part of the foreshock cavity structure.

[21] **Acknowledgments.** Work for this project was supported by NSF Grant AGS-1007449 and NASA's THEMIS mission. DRC's work was supported by CONACYT through a PhD scholarship.

References

Asbridge, J. R., S. J. Bame, and I. B. Strong (1968), Outward flow of protons from the Earth's bow shock, *J. Geophys. Res.*, *73*, 5777.

Billingham L., S. J. Schwartz, and D. G. Sibeck (2008), The statistics of foreshock cavities: results of a Cluster survey, *Ann. Geophys.*, *26*, 3653–3667.

Blanco-Cano, X., N. Omidi, and C. T. Russell (2006), Macro-structure of collisionless bow shocks: 2. Wave properties, *J. Geophys. Res.*, *111*, A10, doi:10.1029/2005JA01142.

Blanco-Cano, X., N. Omidi, and C. T. Russell (2009), Global hybrid simulations: Foreshock waves and cavitons under radial IMF geometry, *J. Geophys. Res.*, *114*, A01216, doi:10.1029/2008JA013406.

Blanco-Cano, X., P. Kajdič, N. Omidi, and C. T. Russell (2011), Foreshock cavitons for different interplanetary magnetic field geometries: Simulations and observations, *J. Geophys. Res.*, *116*, A09101, doi:10.1029/2010JA016413.

Bonifazi, C., A. Egidi, G. Moreno, and S. Orsini (1980a), Backstreaming ions outside the Earth's bow shock and their interaction with the solar wind, *J. Geophys. Res.*, *85*, 3461.

Bonifazi, C., G. Moreno, A. J. Lazarus, and J. D. Sullivan (1980b), Deceleration of the solar wind in the Earth's foreshock region: ISEE 2 and IMP 8 observations, *J. Geophys. Res.*, *85*, 6031.

Fuselier, S. A. (1995), Ion distributions in the Earth's foreshock upstream from the bow shock, in Physics of Collisionless Shocks, edited by C. T. Russell, 43 pp., Advances in Space Research, Pergamon.

Gosling J. T., J. R. Asbridge, S. J. Bame, G. Paschmann, and N. Sckopke (1978), Observations of two distinct populations of bow shock ions in the upstream solar wind, *J. Geophys. Res.*, *5*, 957.

Greenstadt, E. W., et al. (1968), Strong, correlated magnetic field and plasma observations of the Earth's bow shock, *J. Geophys. Res.*, *73*, 51.

Greenstadt, E. W., C. T. Russell, and M. Hoppe (1980), Magnetic field orientation and suprathermal ion streams in the Earth's foreshock, *J. Geophys. Res.*, *85*, 3473.

Hoppe M. M., C. T. Russell, L. A. Frank, T. E. Eastman, and E. W. Greenstadt (1981), Upstream hydromagnetic waves and their association with backstreaming ion populations ISEE 1 and 2 observations, *J. Geophys. Res.*, *86*, 4471–4492.

Kajdič, P., X. Blanco-Cano, N. Omidi, and C. T. Russell (2011), Multispacecraft study of foreshock cavitons upstream of the quasi-parallel Earth's bow shock, *Planet. Space Sci.*, *59*, 705–714, doi:10.1016/j.pss.2011. 02.005.

Mazelle, C., et al. (2003), Production of gyrating ions from nonlinear wave-particle interaction upstream from the Earth's bow shock: A case study from Cluster-CIS, *Planet. Space Sci.*, *51*, 785–795, doi:10.1016/j.pss.2003.05.002.

Omidi, N., and D. Sibeck (2007), Formation of hot flow anomalies and solitary shocks, *J. Geophys. Res.*, *112*, A01203, doi:10.1029/2006JA011663.

Omidi, N., et al. (2004), Dipolar magnetospheres and their characterization as a function of magnetic moment, *Adv. Space Res.*, *33*(11), 1996.

Omidi, N., X. Blanco-Cano, and C. T. Russell (2005), Macro-structure of collisionless bow shocks: 1. Scale lengths, *J. Geophys. Res.*, *110*, A12212, doi:10.1029/2005JA011169.

Omidi, N., X. Blanco-Cano, C. Russell, and H. Karimabadi (2006), Global hybrid simulations of solar wind interaction with Mercury: Magnetospheric boundaries, *Adv. Space Res.*, doi:10.1016/j.asr.2005.11.019.

Omidi, N., D. Sibeck, and X. Blanco-Cano (2009), The foreshock compressional boundary, *J. Geophys. Res.*, *114*, A08205, doi:10.1029/2008JA013950.

Omidi, N., J. Eastwood, and D. Sibeck (2010), Foreshock bubbles and their global magnetospheric impacts, *J. Geophys. Res.*, *115*, A06204, doi:10.1029/2009JA014828.

Paschmann, G., et al. (1979), Association of low frequency waves with suprathermal ions in the upstream solar wind, *Geophys. Res. Lett.*, *6*, 209.

Rojas-Castillo, D., X. Blanco-Cano, P. Kajdic, and N. Omidi (2012), Foreshock compressional boundaries observed by Cluster, *J. Geophys. Res.*, *118*, doi:10.1029/2011JA017385, in press.

Russell, C. T., and M. Hoppe (1983), Upstream waves and particles, *Space Sci. Rev.*, *34*, 155.

Sibeck, D. G., et al. (2002), Wind observations of foreshock cavities: A case study, *J. Geophys. Res.*, *107*, 1271, doi:10.1029/2001JA007539.

Sibeck, D. G., N. Omidi, I. Dandouras, and E. Lucek (2008), On the edge of the foreshock: model-data comparisons, *Ann. Geophys.*, *26*, 1539.

Skadron, G., R. D. Holdaway, and M. Scholer (1986), Perturbation of the solar wind in a model terrestrial foreshock, *J. Geophys. Res.*, *91*, 8798.

Skadron, G., R. D. Holdaway, and M. A. Lee (1988), Formation of the wave compressional boundary in the Earth's foreshock, *J. Geophys. Res.*, *93*, 11354.

Turner, D. L., N. Omidi, D. G. Sibeck and V. Angelopoulos (2012), First observations of foreshock bubbles upstream of Earth's bow shock: Characteristics and comparing to HFAs, *J. Geophys. Res.*, submitted.

Winske, D. and N. Omidi (1993), Hybrid codes: Methods and applications, in Computer Space Plasma Physics: Simulation Techniques and Software, edited by H. Matsumoto and Y. Omura, 103 pp., Terra Scientific, Tokyo, Japan.

Winske, D., and N. Omidi (1996), A nonspecialist's guide to kinetic simulations of space plasmas, *J. Geophys. Res.*, *101*, 17287.